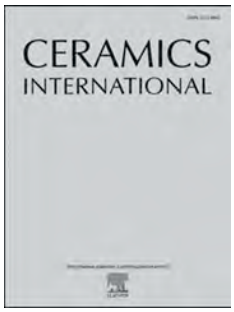

Microwave dielectric properties, microstructure, and bond energy of $Zn_{3-x}Co_xB_2O_6$ low temperature fired ceramics

Maofeng Zhong, Xiaoli Tang, Yuanxun Li, Yulan Jing, Hua Su

PII: S0272-8842(20)31124-X

DOI: https://doi.org/10.1016/j.ceramint.2020.04.180

Reference: CERI 24977

To appear in: *Ceramics International*

Received Date: 19 March 2020

Revised Date: 10 April 2020

Accepted Date: 18 April 2020

Please cite this article as: M. Zhong, X. Tang, Y. Li, Y. Jing, H. Su, Microwave dielectric properties, microstructure, and bond energy of $Zn_{3-x}Co_xB_2O_6$ low temperature fired ceramics, *Ceramics International* (2020), doi: https://doi.org/10.1016/j.ceramint.2020.04.180.

Microwave dielectric properties, microstructure, and bond energy of $Zn_{3-x}Co_xB_2O_6$ low temperature fired ceramics

Maofeng Zhong[1], Xiaoli Tang[1], Yuanxun Li[1,2], Yulan Jing[1], Hua Su[1,2*]

[1]*State Key Laboratory of Electronic Thin Films and Integrated Devices, University of Electronic Science and Technology of China, Chengdu, 610054, China*

[2]*Jiangxi Guo Chuang Industrial Park Development Co., Ltd, Ganzhou, China.*

**Corresponding author: uestcsh@163.com*

Abstract

Low temperature co-fired ceramics (LTCCs) technology plays an important role in modern wireless communication. $Zn_{3-x}Co_xB_2O_6$ (x=0−0.25) low temperature fired ceramics were synthesized via traditional solid-state reaction method. Influences of Co^{2+} substitution on crystal phase composition, grain size, grain morphology, microwave dielectric properties, bond energy, and bond valence were investigated in detail. X-ray diffraction analysis indicated that the major phase of the ceramics was monoclinic $Zn_3(BO_3)_2$. Solid solution was formed with Co^{2+} substituted for Zn^{2+} because no individual phase that contained Co was observed. An increase in the amount of Co^{2+} substitution changed average grain sizes, and regrowth of grains were observed with Co^{2+} substitution. Appropriate amount of Co^{2+} substitution improved densification. With changes in Co^{2+} substitution, bond energy of major phase and average bond valence of B-O were positively correlated to temperature coefficient of resonant frequency. The $Zn_{2.927}Co_{0.075}B_2O_6$ ceramic sintered at 875 °C for 4 h exhibited excellent microwave properties with ε_r=6.79, $Q\times f$=140402 GHz, and τ_f=-87.42 ppm/°C. This ceramic is regarded as candidate for LTCC applications.

Keywords: *Microwave dielectric properties; LTCC; microstructure; bond energy*

1. Introduction

Microwave dielectric ceramics are indispensable in the development of wireless communication; specifically, these ceramics are commonly used as resonators and capacitors [1]-3]. With further development in wireless communication, new demands have been proposed for microwave dielectric ceramics: miniaturization, multifunction, high reliability, and low dielectric loss at high frequency. Low temperature co-fired ceramics (LTCCs) and corresponding technologies that meet these demands, are also beneficial for radio frequency (RF) microwave and millimeter-wave circuits [4]. LTCCs are used to package passive and active components into multilayer structures to achieve the characteristics of miniaturization and multifunction. Ag is usually used as an electrode in the LTCC multilayer because of its low conductor loss and low cost. To co-fire a ceramic with Ag, the sintering temperature of the ceramic must usually be below 950 °C. A low relative dielectric constant (ε_r) is required for LTCCs in substrate applications because the relationship between ε_r and propagation delay time (T_d) is: $T_d=L\sqrt{\varepsilon_r}/c$ [5], where L is the traveling distance of the signal and c is the speed of light. Low dielectric loss of LTCCs is an important feature and it is related to high efficiency and low noise in devices [6]. Moreover, the temperature coefficient of the resonant frequency (τ_f) of LTCCs is a measure of the temperature stability of the resonant frequency, which is required near zero for practical applications.

Not every microwave dielectric ceramic is suitable for LTCC technology. For example, the densification temperature is as high as 1340 °C for Zn_2SiO_4 [7] and 1400 °C for Mg_2SiO_4 [8], and these sintering temperatures are extremely high for LTCC applications. Glasses, oxides, and fluorides, which have low melting points, are usually used as sintering aids to reduce the sintering temperature of these ceramics with low

dielectric loss [6],9],10]. Furthermore, ceramics without sintering aids, such as $Sr_2NaMg_2V_3O_{12}$, $La_2Zr_3(MoO_4)_9$, and $LiNiPO_4$, have also been investigated in recent years [11]−13]. Wu et al.[14] first reported the microwave dielectric properties of the $Zn_3B_2O_6$ ceramic sintered at 925 °C for 4 h: ε_r=6.7, $Q\times f$=58500 GHz, and τ_f=-58 ppm/°C. $Zn_3B_2O_6$ has an innate low sintering temperature and excellent microwave dielectric properties, and thus, it is suitable for LTCC applications. Previous research has reported that Co^{2+} substitution is an efficient means of increasing relative density and $Q\times f$, and decreasing sintering temperature[15]−18]. Moreover, the effective radius of Zn^{2+} is 0.60 Å, and that of Co^{2+} is 0.58 Å when their coordination number (CN) is 4 [19].

On the basis of the above information, $Zn_{3-x}Co_xB_2O_6$ (x=0-0.25) ceramics without sintering aids were synthesized via the solid-state reaction method in this work. The influences of substituting Co^{2+} for Zn^{2+} on crystal phase, microstructure, densification, and microwave dielectric properties of $Zn_{3-x}Co_xB_2O_6$ ceramics were investigated. The relationship between crystal phase, microstructure, densification, bond energy, bond valence, and microwave dielectric properties of $Zn_{3-x}Co_xB_2O_6$ ceramics were investigated in detail.

2. Experimental procedure

Samples of $Zn_{3-x}Co_xB_2O_6$ (x=0−0.25) ceramics were prepared via the solid-state reaction method. Analytically pure ZnO (99.0%, Ke Long chemical factory in China), CoO (99.0%, Ke Long chemical factory in China), and H_3BO_3 (99.5%, Ke Long chemical factory in China) were used as raw materials. The loss of B_2O_3 during calcination was compensated for 12 wt.% excess H_3BO_3 in the first step of weighing the raw material [14]. The mixtures were weighted according to the compositions and

milled with deionized water and zirconia balls in nylon containers for 4 h. The mixed slurries were then dried in an oven respectively and then calcined at 875 °C for 4 h. The calcined materials were remilled for 4 h. The wet materials were dried and mixed with polyvinyl alcohol binder (12 wt.%). Samples were then pressed into cylinders with 12 mm in diameter and 6 mm in height at 100 MPa. The raw cylinders were sintered at 850-900 °C for 4 h to obtain the final samples that were used for subsequent tests.

Crystal phases of the ceramics were identified via a X-ray diffractometer (Rigaku MinFlex 600) with a scanning speed of 4°/min. Crystal structure parameters of the samples were obtained via refinements of X-ray diffraction (XRD) data using FullProf software. The bond energy and bond valence were calculated from the refined XRD data. A scanning electron microscope (SEM: JEOL JSM-6490LV) with an acceleration voltage of 20 kV, was used to observe grain sizes and microstructure of the sintered ceramics. Archimedes' method was used to measure bulk densities of the samples. Microwave dielectric properties of the ceramics were measured via the Hakki-Coleman dielectric resonator method using a vector network analyzer (Agilent Technologies, N5230A, 300 kHz~20 GHz) [20]. The temperature coefficient of the resonant frequency (τ_f) was determined using Equation (1):

$$\tau_f = \frac{f_2 - f_1}{f_1(T_2 - T_1)} \times 10^6 \text{ (ppm/°C)} \quad (1)$$

where f_1 and f_2 are the resonant frequencies measured at temperatures T_1 and T_2, respectively.

3. Results and discussion

Fig. 1

The $Zn_{3-x}Co_xB_2O_6$ (x=0-0.25) ceramics sintered at 875 °C present a major phase ($Zn_3(BO_3)_2$, ICSD #14240) and a minor phase ($Zn_4O(B_6O_{12})$, ICSD #34085), as shown

in Fig. 1(a). The standard XRD patterns of the two phases are based on the ICSD data and their curves are calculated using Mercury software. The main diffraction peaks are in the range of 20°-50°, and some of the indexes of diffraction are labeled in Fig. 1. Substituting Co^{2+} for Zn^{2+} did not introduce any new phase containing Co, and this fact indicated that Co^{2+} replaced the position of Zn^{2+} and formed a solid solution in $Zn_{3-x}Co_xB_2O_6$ (x=0-0.25) ceramics. The similarity in the values of the effective ion radii of Zn^{2+} and Co^{2+} was the necessary condition for forming the solid solution. In addition, the diffraction peak (211) of the minor phase is not observed until substitution of Co^{2+} is increased to 0.15 mole, as seen in Fig. 1(b), and this demonstrated that $Zn_3(BO_3)_2$ formed a solid solution with $Zn_4O(B_6O_{12})$ when $x \leq 0.075$ and that further substitution of Co^{2+} reduced the compatibility on structure between the two phases. The intensity of the diffraction peak (310) of the minor phase is stable, as seen in Fig. 1(c), and this indicated that Co^{2+} substitution did not obviously change the weight percentage of the $Zn_4O(B_6O_{12})$ phase in the samples.

Fig. 2

XRD patterns were refined using FullProf software with the Rietveld method [21]. Characteristics of the crystal structure, lattice parameters (*a*, *b*, *c*), and volume of the unit cell (*Vc*) were obtained from the refinements of $Zn_{3-x}Co_xB_2O_6$ (x=0-0.25) ceramics sintered at 875 °C. Monoclinic structure with the space group of I 1 2/c 1 for $Zn_3(BO_3)_2$ and cubic structure with the space group of I -4 3 m for $Zn_4O(B_6O_{12})$ were used as models for XRD refinements. Details of the models were based on the standard PDF cards ICSD #14240 and ICSD #34085. Moreover, $\alpha=\gamma=90°$ in the monoclinic structure. And $a=b=c$, $\alpha=\beta=\gamma=90°$ in the cubic structure. The results of the XRD refinements can be seen in Fig. 2 and the refinements are summarized in Table 1. The values of χ^2 were

less than 2, which showed that the refinements were reliable. The lattice parameters changed slightly with an increase in Co^{2+} substitution, and this indicated that $Zn_{3-x}Co_xB_2O_6$ (x=0−0.25) ceramics sintered at 875 °C were stable on the structure. Furthermore, the weight percentages of $Zn_3(BO_3)_2$ and $Zn_4O(B_6O_{12})$ changed with a change in x, and the weight percentage of $Zn_4O(B_6O_{12})$ was maximized at x=0.075.

Fig. 3

The crystal structure of the major phase ($Zn_3(BO_3)_2$) is shown in Fig. 3; this was obtained from the result of XRD refinement for the $Zn_{2.925}Co_{0.075}B_2O_6$ ceramic, which was sintered at 875 °C. In this sample, the unit cell of monoclinic phase $Zn_3(BO_3)_2$ included 8 molecules of $Zn_3B_2O_6$, with β=97.40376°, a=23.44124 Å, b=5.04233 Å, and c=8.38215 Å. Zn^{2+}, B^{3+}, and O^{2-} formed tetrahedral [ZnO_4] and triangular [BO_3] connected though the vertex O^{2-}. Moreover, on the basis of the principle of charge conservation, one O^{2+} connected one triangle of [BO_3] and two tetrahedra of [ZnO_4] in the crystal phase $Zn_3(BO_3)_2$. In a practical sample, because some Co^{2+} was substituted for Zn^{2+}, Co^{2+} replaced some of Zn^{2+} in the crystal structure. The crystal structure remained stable even when the amount of substitution reached to 0.25 mole, as seen from the analysis of the XRD patterns.

Fig. 4

Fig. 5

Microstructure and grain morphology of the ceramics are related to the microwave dielectric properties [23]. The microstructure, grain size, and grain morphology of $Zn_{3-x}Co_xB_2O_6$ (x=0−0.25) ceramics sintered at 875 °C were observed via SEM, as seen in Fig. 4. The average grain sizes and their standard deviations are showed in Fig. 5. Grain boundaries of all samples were apparent, but the morphology of the grains

changed with an increase in Co^{2+} substitution. With an increase in Co^{2+} substitution from 0 mole to 0.05 mole, the grains of the ceramics regrew, as seen in Fig. 4(a)-(c). The morphology of the grains changed obviously; specifically, some irregular grains appeared in the range of $0.025 \leq x \leq 0.05$. Thus, it could be concluded that substituting an appropriate amount of Co^{2+} for Zn^{2+} promoted the regrowth of grains in $Zn_{3-x}Co_xB_2O_6$ ceramics. Furthermore, the average grain size decreased from 3.79 μm at x=0 to 2.77 μm at x=0.05, and the decrease in the corresponding standard deviation of grain size also supported this conclusion. The grain morphology became regular again, and grains grew closely when x reached 0.075, as seen in Fig. 4(d). With a further increase in the amount of Co^{2+} substitution to 0.25 mole, the average grain size increased to 4.08 μm, and their grain boundaries tended to be blurry.

Fig. 6

The bulk density and relative density of the samples are shown in Fig. 6. The theoretical density of $Zn_{3-x}Co_xB_2O_6$ (x=0−0.25) ceramics was assumed to be equal for samples at different sintering temperatures. Moreover, the theoretical density (ρ_{th}) and relative density (ρ_r) of the samples were calculated using Equations (2) and (3), as shown below:

$$\rho_{th} = \frac{ZA}{V_c N_A}, \tag{2}$$

$$\rho_r = \frac{\sum w_i}{\sum \frac{w_i}{\rho_i}}, \tag{3}$$

where N_A, V_c, A, and Z are the Avogadro's constant (mol^{-1}), the volume of unit cell, the molar molecular weight (g/mol), and the number of molecules in a unit cell, respectively. Also, w_i and ρ_i were the weight percentage and theoretical density of phase i respectively. Values of V_c were derived from the results of XRD refinements. Bulk

densities of the samples varied between 3.785 g/cm^3 and 4.067 g/cm^3, and relative densities varied between 89.98% and 95.98%. The densest sample was the $Zn_{2.925}Co_{0.075}B_2O_6$ ceramic sintered at 875 °C, with a bulk density of 4.067 g/cm^3 and relative density of 95.98%. The variations in bulk density and relative density were similar because of their similar values of the theoretical density of $Zn_{3-x}Co_xB_2O_6$ ceramics with different values of x. The relationship between porosity (P) and relative density (ρ_r) is P=1-ρ_r. As seen in Fig. 6(b), an optimal amount of substituted Co^{2+} enabled the ceramics to reach maximal relative density, and the optimal amount varied at different sintering temperatures. Higher sintering temperature corresponded to a smaller optimal amount of substituted Co^{2+} for $Zn_{3-x}Co_xB_2O_6$ (x=0-0.25) ceramics sintered at 850-900 °C. This phenomenon indicated that an appropriate amount of Co^{2+} substitution reduced porosity of the ceramics subjected to the same sintering temperature, and this influence increased when the sintering temperature was higher.

Fig. 7

Relative dielectric constants (ε_r) of ceramics mainly depend on crystal phase composition and porosity [24]-25]. ε_r values of $Zn_{3-x}Co_xB_2O_6$ (x=0−0.25) ceramics sintered at 850-900 °C are shown in Fig. 7(a). Phase compositions of $Zn_{3-x}Co_xB_2O_6$ (x=0−0.25) ceramics sintered at 875 °C could be observed from the results of XRD refinements; the weight percentages of the major phase and minor phase were slightly changed. In this situation, changes in the weight percentage of the phase composition were not the dominant factor that influenced changes in ε_r. Furthermore, the same changes were observed between the relative density and ε_r. Therefore, values of ε_r for $Zn_{3-x}Co_xB_2O_6$ ceramics were mainly influenced by relative density or porosity. The value of ε_r for the densest $Zn_{2.925}Co_{0.075}B_2O_6$ ceramic sintered at 875 °C was 6.79.

Equation (4) was used to calculated the value of ε_r for the pure ceramic without porosity [25]:

$$\varepsilon_r=\varepsilon_m\left(1-\frac{3P(\varepsilon_m-1)}{2\varepsilon_m+1}\right) \quad (4)$$

where ε_r, P, and ε_m are the measured relative dielectric constant, fractional porosity, and calculated ε_r value of the pure ceramic respectively. The value of ε_r for the pure $Zn_{2.925}Co_{0.075}B_2O_6$ ceramic sintered at 875 °C was calculated to be 7.14.

Dielectric loss of microwave dielectric ceramics is related to intrinsic loss (such as phase composition and crystal structure) and extrinsic loss (such as porosity and phase crystallization) [26],27]. $Q\times f$ was used to measure dielectric loss of the ceramics, and the results are shown in Fig. 7(b). Relative density showed the same variation with $Q\times f$ for $Zn_{3-x}Co_xB_2O_6$ (x=0−0.25) ceramics, and this fact indicated that porosity was the dominant factor that influenced dielectric loss of the ceramics. In other words, an appropriate amount of Co^{2+} substitution enhanced densification and reduced the dielectric loss of the $Zn_{3-x}Co_xB_2O_6$ (x=0−0.25) ceramics. $Q\times f$ value of the $Zn_{2.925}Co_{0.075}B_2O_6$ ceramic sintered at 875 °C was much larger than that of the other samples sintered at the same temperature. This phenomenon might contribute to the phase composition and corresponding crystal structure. As discussed regarding the XRD patterns shown in Fig. 1(a), $Zn_3(BO_3)_2$ formed a solid solution with $Zn_4O(B_6O_{12})$ when $x\leq0.075$, and further Co^{2+} substitution reduced their compatibility on the structure. The $Zn_{2.925}Co_{0.075}B_2O_6$ ceramic sintered at 875 °C contained the maximal weight percentage of $Zn_4O(B_6O_{12})$, and there was complete compatibility on the structure between the two phases. Therefore, the compatibility on the crystal structure and high densification increased the $Q\times f$ to 140402 GHz for the $Zn_{2.925}Co_{0.075}B_2O_6$ ceramic sintered at 875 °C.

$Zn_3(BO_3)_2$ was the major phase in $Zn_{3-x}Co_xB_2O_6$ (x=0-0.25) ceramics. Total bond

energy of the $Zn_3(BO_3)_2$ phase in $Zn_{3-x}Co_xB_2O_6$ (x=0-0.25) ceramics sintered at 875 °C was calculated strictly according to the theory of Sanderson [28],29]. All data used to calculated the bond energy could be found in Ref. [29] and Table 2. Bond energy (E_b) of a single bond contains nonpolar covalent bond energy (E_c) and polar covalent bond energy (E_i):

$$E_b = t_c E_c + t_i E_i \tag{5}$$

$$1 = t_c + t_i \tag{6}$$

where t_c, and t_i are the covalent and ionic blending coefficients respectively. The partial charges of the atoms that constitute the chemical bond were used to calculate the value of t_i according to the following equation:

$$t_i = \frac{|C_{PA} - C_{PB}|}{2} \tag{7}$$

where C_{PA} and C_{PB} are the partial charges of atoms A and B respectively. The electronegativity of the molecule and atoms that constituted the chemical bond were used to calculate the partial charge according to the following equation:

$$C_{Pi} = \frac{S_m - S_i}{\Delta S_i} \tag{8}$$

where C_{Pi}, S_m, and S_i are the partial charge of atom i, electronegativity of the molecule that contains the chemical bond, and the electronegativity of atom i respectively. Polyhedra of $[Zn(1)O_4]$, $[Zn(2)O_4]$, $[Zn(3)O_4]$, $[B(1)O_3]$, and $[B(2)O_3]$ were considered to be 5 styles of molecules that formed the $Zn_3(BO_3)_2$ phase. ΔS_i is the change in the complete loss of an electron. S_m is simply the geometric mean of the electronegativity of all the atoms that constitute the molecule, and it was calculated using the following Equation:

$$S_m = \sqrt[n]{\prod_{j=1}^{n} S_j} \tag{9}$$

where S_j is the electronegativity of atom j, and n is the number of atoms that form the molecule. Moreover, E_c and E_i were calculated using Equations (10) and (11):

$$E_i = \frac{33200}{R_o} \tag{10}$$

$$E_c = \frac{(R_A+R_B)(E_{A-A}E_{B-B})^{1/2}}{R_o} \tag{11}$$

where R_o, R_A, and R_B are respectively the bond length between atoms A and B, nonpolar covalent radii of atom A, and nonpolar covalent radii of atom B. Bond length (pm) corresponds to E_i in kcal/mol. E_{A-A} and E_{B-B} are defined as homonuclear bond energies of atom A and B, respectively. Particularly, E_{Zn-Zn}=35.8 kcal/mol, E_{B-B}=76.7 kcal/mol, E_{O-O}=104 kcal/mol. The bond energy of a polyhedra is the sum of the bond energies of all of the individual bonds that form the polyhedra. Furthermore, the total bond energies of the $Zn_3(BO_3)_2$ phase, that is, the total energies of the five types of polyhedra in $Zn_{3-x}Co_xB_2O_6$ (x=0−0.25) ceramics, were calculated to compare with the value of τ_f, as seen in Fig. 8.

Fig. 8

It has been observed in previous research that bond valence was related to τ_f [9],30]. [BO_3] triangles are the basic framework in $Zn_{3-x}Co_xB_2O_6$ (x=0−0.25) ceramics. Therefore, the average bond valence of B-O was calculated using Equations (12) and (13) [31]:

$$d_{ij} = R_{ij} - b \ln v_{ij} \tag{12}$$

$$V_a = \frac{\sum v_{ij}}{n} \tag{13}$$

where d_{ij}, R_{ij}, and v_{ij} are the bond length between atoms i and j, bond valence parameter, bond valence of atoms i and j, respectively. V_a is the average bond valence, and n is the number of bonds included in the calculation. According to Ref. [31], b=0.37 Å, and

R_{B-O}=1.37 Å. There were six types of B-O bonds in $Zn_3(BO_3)_2$, and bond length values are shown in Table 2. The average bond valence of B-O was simply the average of the six types of B-O bond valence. Calculated average bond valences of B-O for the $Zn_3(BO_3)_2$ phase in $Zn_{3-x}Co_xB_2O_6$ ceramics sintered at 875 °C are shown in Fig. 8.

The value of τ_f is mainly influenced by phase composition, the linear expansion coefficient (α), and the temperature coefficient of the dielectric constant (α_ε) [22],23]:

$$\tau_f = -(\alpha + \frac{1}{2}\alpha_\varepsilon) \quad (14)$$

Bond energy is related to the stability of the crystal structure of the ceramics, and therefore, bond energy is related to τ_f. B-site bond valence is related to the temperature coefficient of the dielectric constant, and according to Equation (14), B-site bond valence is related to τ_f [17]. Phase composition was obtained from results of XRD refinements. There was no obviously relationship between the percentage of the $Zn_4O(B_6O_{12})$ phase and the value of τ_f due to the slight change in the phase composition. Moreover, bond energy of $Zn_3(BO_3)_2$ and average bond valence of B-O triangles were observed to be positively correlated to τ_f, as shown in Fig. 8. Therefore, the major phase $Zn_3(BO_3)_2$ determined τ_f values of the $Zn_{3-x}Co_xB_2O_6$ (x=0−0.25) ceramics. τ_f values of the $Zn_{3-x}Co_xB_2O_6$ ceramics sintered at 875 °C varied from −62.49ppm/°C to −87.42ppm/°C. An appropriate amount of Co^{2+} substitution reduced the bond energy of $Zn_3(BO_3)_2$ to 8146 kJ/mol at x=0.075, and also resulted in a relatively large negative value of τ_f (−87.42 ppm/°C), and this indicated that low bond energy corresponded to low stability on the structure of the ceramics. Similarly, the conclusion that smaller average bond valence of B-O corresponded to larger negative τ_f for $Zn_{3-x}Co_xB_2O_6$ ceramics sintered at 875 °C was made. Furthermore, τ_f should be near zero for practical application, and some methods for adjusting τ_f have been investigated. These methods

included substituting ions (Cu^{2+},Ti^{4+}) [27],32] or compensating with other materials that have large positive values of τ_f [21],33].

4. Conclusions

$Zn_{3-x}Co_xB_2O_6$ (x=0-0.25) ceramics sintered at 850-900 °C were prepared via the traditional solid-state reaction method. A major phase $Zn_3(BO_3)_2$ and minor phase $Zn_4O(B_6O_{12})$ constituted the crystal phase of the ceramics. Co^{2+} substitution promoted the regrowth of grains and changes in grain size. An appropriate amount of Co^{2+} substitution increased relative density and reduced dielectric loss. The $Zn_{2.925}Co_{0.075}B_2O_6$ ceramic sintered at 875 °C was the densest sample. The value of $Q\times f$ was closely related to relative density, phase composition, and crystal structure. Bond energy of $Zn_3(BO_3)_2$ and average bond valence of B-O were calculated and presented a positive correlation with τ_f. The $Zn_{2.927}Co_{0.075}B_2O_6$ ceramic sintered at 875 °C for 4 h exhibited excellent microwave properties with ε_r=6.79, $Q\times f$=140402 GHz, and τ_f=−87.42 ppm/°C. Thus, the ceramic was regarded as a potential LTCC material.

Acknowledgements

This work was supported by the National Natural Science Foundation of China under Grant Nos. 61771104, U1809215, and 61871069.

References

[1] X.Q. Song, W.Z. Lu, X.C. Wang, X.H. Wang, G.F. Fan, R. Muhammad, W. Lei, Sintering behaviour and microwave dielectric properties of $BaAl_{2-2x}(ZnSi)_xSi_2O_8$ ceramics, J. Eur. Ceram. Soc. 38 (2018) 1529–1534. https://doi.org/10.1016/j.jeurceramsoc.2017.10.053.

[2] T. Okawa, H. Utaki, T. Takada, The application of microwave ceramics, Proc. 1994 IEEE Int. Symp. Appl. Ferroelectr. (1991) 367–371.

https://doi.org/10.1109/ISAF.1994.522379.

[3] A. Manan, I. Qazi, Dielectric Properties of Ceramics for Microwave and Millimeterwave Applications, Int. Conf. Aerosp. Sci. Eng. (ICASE). IEEE. 2 (2013) 1–7. https://doi.org/10.1109/ICASE.2013.6785564.

[4] I. Wolff, C. Günner, J. Kassner, R. Kulke, P. Uhlig, New heights for satellites, IEEE Microw. Mag. 19 (2018) 36–47. https://doi.org/10.1109/MMM.2017.2759599.

[5] B. Schwartz, Review of multilayer ceramics for microelectronic packaging, J. Phys. Chem. Solids. 45 (1984) 1051–1068. https://doi.org/10.1016/0022-3697(84)90048-9.

[6] M.T. Sebastian, H. Jantunen, Low loss dielectric materials for LTCC applications: A review, Int. Mater. Rev. 53 (2008) 57–90. https://doi.org/10.1179/174328008X277524.

[7] Y. Guo, H. Ohsato, K.I. Kakimoto, Characterization and dielectric behavior of willemite and TiO_2-doped willemite ceramics at millimeter-wave frequency, J. Eur. Ceram. Soc. 26 (2006) 1827–1830. https://doi.org/10.1016/j.jeurceramsoc.2005.09.008.

[8] T. Tsunooka, M. Androu, Y. Higashida, H. Sugiura, H. Ohsato, Effects of TiO_2 on sinterability and dielectric properties of high-Q forsterite ceramics, J. Eur. Ceram. Soc. 23 (2003) 2573–2578. https://doi.org/10.1016/S0955-2219(03)00177-8.

[9] X.Q. Song, K. Du, J. Li, X.K. Lan, W.Z. Lu, X.H. Wang, W. Lei, Low-fired fluoride microwave dielectric ceramics with low dielectric loss, Ceram. Int. 45 (2019) 279–286. https://doi.org/10.1016/j.ceramint.2018.09.164.

[10] Y. Lai, H. Su, G. Wang, X. Tang, X. Huang, X. Liang, H. Zhang, Y. Li, K. Huang, X.R. Wang, Low-temperature sintering of microwave ceramics with high Qf values

through LiF addition, J. Am. Ceram. Soc. 102 (2019) 1893–1903. https://doi.org/10.1111/jace.16086.

[11] H. Xiang, L. Fang, X. Jiang, Y. Tang, C. Li, A Novel Temperature Stable Microwave Dielectric Ceramic with Garnet Structure: $Sr_2NaMg_2V_3O_{12}$, J. Am. Ceram. Soc. 99 (2016) 399–401. https://doi.org/10.1111/jace.14034.

[12] W. Liu, R. Zuo, A novel low-temperature firable $La_2Zr_3(MoO_4)_9$ microwave dielectric ceramic, J. Eur. Ceram. Soc. 38 (2018) 339–342. https://doi.org/10.1016/j.jeurceramsoc.2017.08.023.

[13] P. Zhang, S. Wu, M. Xiao, The microwave dielectric properties and crystal structure of low temperature sintering $LiNiPO_4$ ceramics, J. Eur. Ceram. Soc. 38 (2018) 4433–4439. https://doi.org/10.1016/j.jeurceramsoc.2018.05.040.

[14] X.G. Wu, H. Wang, Y.H. Chen, D. Zhou, Synthesis and microwave dielectric properties of $Zn_3B_2O_6$ Ceramics for substrate application, J. Am. Ceram. Soc. 95 (2012) 1793–1795. https://doi.org/10.1111/j.1551-2916.2012.05192.x.

[15] C.L. Huang, J.Y. Chen, Phase relation and microwave dielectric properties of $(Zn_{1-x}Co_x)Ta_2O_6$ system, J. Am. Ceram. Soc. 93 (2010) 1248–1251. https://doi.org/10.1111/j.1551-2916.2009.03546.x.

[16] H.W. Chen, H. Su, H.W. Zhang, T.C. Zhou, B.W. Zhang, J.F. Zhang, X.L. Tang, Low-temperature sintering and microwave dielectric properties of $(Zn_{1-x}Co_x)_2SiO_4$ ceramics, Ceram. Int. 40 (2014) 14655–14659. https://doi.org/10.1016/j.ceramint.2014.06.053.

[17] W.R. Yang, P.Z. Huang, C.L. Huang, Microwave dielectric properties of low-loss $(Zn_{1-x}Co_x)_3Nb_2O_8$ ceramics for LTCC applications, J. Alloys Compd. 620 (2015) 18–23. https://doi.org/10.1016/j.jallcom.2014.08.202.

[18] A. Ullah, H. Liu, Z. Pengcheng, H. Hao, J. Iqbal, M. Cao, Z. Yao, A.S. Ahmad, A. Manan, Influence of Co substitution on the phase, microstructure, and microwave dielectric properties of $MgSiO_3$ ceramics, J. Mater. Sci. Mater. Electron. 30 (2019) 6469–6474. https://doi.org/10.1007/s10854-019-00951-8.

[19] R.D. Shannon, Revised effective ionic radii and systematic studies of interatomic distances in halides and chalcogenides, Acta Crystallogr. Sect. A. 32 (1976) 751–767. https://doi.org/10.1107/S0567739476001551.

[20] B.W. Hakki, P.D. Coleman, A Dielectric Resonator Method of Measuring Inductive Capacities in the Millimeter Range, IRE Trans. Microw. Theory Tech. MTT-8 (1960) 402–410. https://doi.org/10.1109/TMTT.1960.1124749.

[21] Y. Lai, C. Hong, L. Jin, X. Tang, H. Zhang, X. Huang, J. Li, H. Su, Temperature stability and high-Qf of low temperature firing Mg_2SiO_4–Li_2TiO_3 microwave dielectric ceramics, Ceram. Int. 43 (2017) 16167–16173. https://doi.org/10.1016/j.ceramint.2017.08.192.

[22] K. Du, X.Q. Song, J. Li, J.M. Wu, W.Z. Lu, X.C. Wang, W. Lei, Optimised phase compositions and improved microwave dielectric properties based on calcium tin silicates, J. Eur. Ceram. Soc. 39 (2019) 340–345. https://doi.org/10.1016/j.jeurceramsoc.2018.10.005.

[23] Y. Lai, X. Tang, H. Zhang, X. Liang, X. Huang, Y. Li, H. Su, Correlation between structure and microwave dielectric properties of low-temperature-fired Mg_2SiO_4 ceramics, Mater. Res. Bull. 99 (2018) 496–502. https://doi.org/10.1016/j.materresbull.2017.11.036.

[24] Y. Imanaka, Multilayered Low Temperature Cofired Ceramics (LTCC) Technology, Springer Sci. Bus. Media. (2005). https://doi.org/10.1007/b101196.

[25] S.J. Penn, N.M. Alford, A. Templeton, X. Wang, M. Xu, M. Reece, K. Schrapel, Effect of Porosity and Grain Size on the Microwave Dielectric Properties of Sintered Alumina, J. Am. Ceram. Soc. 80 (2005) 1885–1888. https://doi.org/10.1111/j.1151-2916.1997.tb03066.x.

[26] B. Tang, Q. Xiang, Z. Fang, X. Zhang, Z. Xiong, H. Li, C. Yuan, S. Zhang, Influence of Cr^{3+} substitution for Mg^{2+} on the crystal structure and microwave dielectric properties of $CaMg_{1-x}Cr_{2x/3}Si_2O_6$ ceramics, Ceram. Int. 45 (2019) 11484–11490. https://doi.org/10.1016/j.ceramint.2019.03.016.

[27] Y. Lai, X. Tang, X. Huang, H. Zhang, X. Liang, J. Li, H. Su, Phase composition, crystal structure and microwave dielectric properties of $Mg_{2-x}Cu_xSiO_4$ ceramics, J. Eur. Ceram. Soc. 38 (2018) 1508–1516. https://doi.org/10.1016/j.jeurceramsoc.2017.10.035.

[28] R.T. SANDERSON, MULTIPLE AND SINGLE BOND ENERGIES IN INORGANIC MOLECULES, J. Inorg. Nucl. Chem. 30 (1968) 375–393. https://doi.org/10.1016/0022-1902(68)80464-6.

[29] R.T. Sanderson, Electronegativity and Bond Energy, J. Am. Chem. Soc. 105 (1983) 2259–2261. https://doi.org/10.1021/ja00346a026.

[30] E.S. Kim, B.S. Chun, R. Freer, R.J. Cernik, Effects of packing fraction and bond valence on microwave dielectric properties of $A^{2+}B^{6+}O_4$ (A^{2+}: Ca, Pb, Ba; B^{6+}: Mo, W) ceramics, J. Eur. Ceram. Soc. 30 (2010) 1731–1736. https://doi.org/10.1016/j.jeurceramsoc.2009.12.018.

[31] M. O'Keeffe, N.E. Brese, Bond□valence parameters for anion□anion bonds in solids, Acta Crystallogr. Sect. B. 48 (1992) 152–154. https://doi.org/10.1107/S0108768191013083.

[32] Y. Zhang, H. Wu, Crystal structure and microwave dielectric properties of $La_2(Zr_{1-x}Ti_x)_3(MoO_4)_9$ ($0 \leq x \leq 0.1$) ceramics, J. Am. Ceram. Soc. 102 (2019) 4092–4102. https://doi.org/10.1111/jace.16268.

[33] H. Nozaki, H. Sakurai, I. Umegaki, E.J. Ansaldo, G.D. Morris, B. Hitti, D.J. Arseneau, D. Andreica, A. Amato, M. Månsson, J. Sugiyama, Structure-microwave property relations in $(Sr_xCa_{(1-x)})_{n+1}Ti_nO_{3n+1}$, J. Eur. Ceram. Soc. 21 (2018) 1723–1726. https://doi.org/10.1016/s0955-2219(01)00102-9.

Figure captions:

Fig. 1 (a) XRD patterns of $Zn_{3-x}Co_xB_2O_6$ (x=0−0.25) ceramics sintered at 875 °C, (b) amplified figure at 2θ = 28.5° – 30.5°, (c) amplified figure at 2θ = 36.5° – 39°.

Fig. 2 Rietveld refinements of $Zn_{3-x}Co_xB_2O_6$ (x=0−0.25) ceramics sintered at 875 °C, (a) x = 0, (b) x = 0.025, (c) x = 0.05, (d) x = 0.075, (e) x = 0.15, (f) x = 0.25.

Fig. 3 The crystal structure of a unite cell of $Zn_3(BO_3)_2$.

Fig. 4 SEM photographs of $Zn_{3-x}Co_xB_2O_6$ (x=0−0.25) ceramics sintered at 875 °C, (a) x = 0, (b) x = 0.025, (c) x = 0.05, (d) x = 0.075, (e) x = 0.15, (f) x = 0.25.

Fig. 5 Statistics of grain sizes of $Zn_{3-x}Co_xB_2O_6$ (x=0−0.25) ceramics sintered at 875 °C, (a) x = 0, (b) x = 0.025, (c) x = 0.05, (d) x = 0.075, (e) x = 0.15, (f) x = 0.25.

Fig. 6 Densification characteristic of $Zn_{3-x}Co_xB_2O_6$ (x=0−0.25) ceramics sintered at 850−900 °C, (a) bulk density, (b) relative density.

Fig. 7 Microwave dielectric properties of $Zn_{3-x}Co_xB_2O_6$ (x=0−0.25) ceramics sintered at 850−900 °C, (a) ε_r, (b) $Q\times f$, (c) τ_f.

Fig. 8 Bond energies of $Zn_3(BO_3)_2$ and average bond valences of B-O contrast to τ_f of $Zn_{3-x}Co_xB_2O_6$ (x = 0 – 0.25) ceramics sintered at 875 °C

Table captions:

Table 1 Parameters of structure and agreement factors of refinements for $Zn_{3-x}Co_xB_2O_6$ (x=0−0.25) ceramics sintered at 875 °C.

Table 2 Bond lengths of $Zn_3(BO_3)_2$ from XRD refinements for $Zn_{3-x}Co_xB_2O_6$ (x=0−0.25) ceramics sintered at 875 °C.

		x = 0	x = 0.025	x = 0.05	x = 0.075	x = 0.15	x = 0.25
$Zn_3B_2O_6$	a (Å)	23.43185	23.46057	23.44825	23.44124	23.43675	23.44434
	b (Å)	5.03966	5.04576	5.04287	5.04233	5.04404	5.04966
	c (Å)	8.37482	8.38577	8.38231	8.38215	8.38755	8.39991
	β (Å)	97.43457	97.41837	97.40679	97.40376	97.39304	97.38065
	V_c (Å^3)	980.656	984.369	982.909	982.496	983.299	986.191
	wt. (%)	96.53	93.59	93.61	92.30	95.69	94.59
$Zn_4O(B_2O_{16})$	a (Å)	7.46698	7.47719	7.47365	7.47241	7.47516	7.47669
	V_c (Å^3)	416.327	418.037	417.445	417.237	417.698	417.953
	wt. (%)	3.47	6.41	6.39	7.70	4.31	5.41
	R_p (%)	5.78	6.18	6.71	7.89	8.67	10.1
	R_{wp} (%)	6.93	7.11	7.70	8.72	8.61	9.03
	R_{exp} (%)	5.43	5.78	6.05	6.48	7.37	8.47
	χ^2	1.63	1.51	1.62	1.81	1.36	1.14

R_p: the profile factor; R_{wp}: weighted profile factor; R_{exp}: expected weighted profile factor; χ^2: reduced chi-square

polyhedron types	Bond types	Bond lengths (pm)					
		x = 0	x = 0.025	x = 0.05	x = 0.075	x = 0.15	x = 0.25
$[Zn(1)O_4]$	Zn(1)-O(1)	199.67600	200.41200	202.17500	200.02200	197.20600	198.76300
	Zn(1)-O(1)	200.06100	201.78500	200.85000	199.63200	200.32600	203.92600
	Zn(1)-O(2)	192.03100	192.73500	194.33600	191.72400	194.15400	193.47300
	Zn(1)-O(3)	196.25200	196.12100	193.51200	194.42000	196.03400	198.39100
$[Zn(2)O_4]$	Zn(2)-O(2)	199.35800	199.82300	199.70400	198.19000	199.95500	199.44700
	Zn(2)-O(3)	192.68500	190.94500	191.11900	192.23200	193.87200	192.63000
	Zn(2)-O(4)	200.50700	199.55200	197.25000	200.41100	198.44600	199.52200
	Zn(2)-O(6)	198.72000	200.61500	201.13400	201.97500	202.74500	203.64800
$[Zn(3)O_4]$	Zn(3)-O(5)	195.12400	197.78700	196.20500	197.06300	196.70700	195.91000
	Zn(3)-O(5)	198.76400	196.71500	197.53700	196.45300	196.01000	194.17000
	Zn(3)-O(4)	194.01100	195.02200	193.90700	196.92200	194.32400	193.54400
	Zn(3)-O(6)	197.07800	196.58700	199.54600	198.71600	197.23800	198.40100
$[B(1)O_3]$	B(1)-O(1)	130.49800	129.23800	130.54200	133.15100	129.58100	121.45100
	B(1)-O(2)	137.67400	138.02000	134.40900	133.25900	137.47100	146.34900
	B(1)-O(3)	136.32700	138.07400	139.80700	144.11500	136.59900	134.76600
$[B(2)O_3]$	B(2)-O(4)	133.75100	136.01400	135.02700	138.10300	135.11800	131.46000
	B(2)-O(5)	137.57500	135.67700	139.77800	131.35100	134.22600	137.01600
	B(2)-O(6)	138.19500	138.39300	134.44200	137.56500	141.10300	142.82900

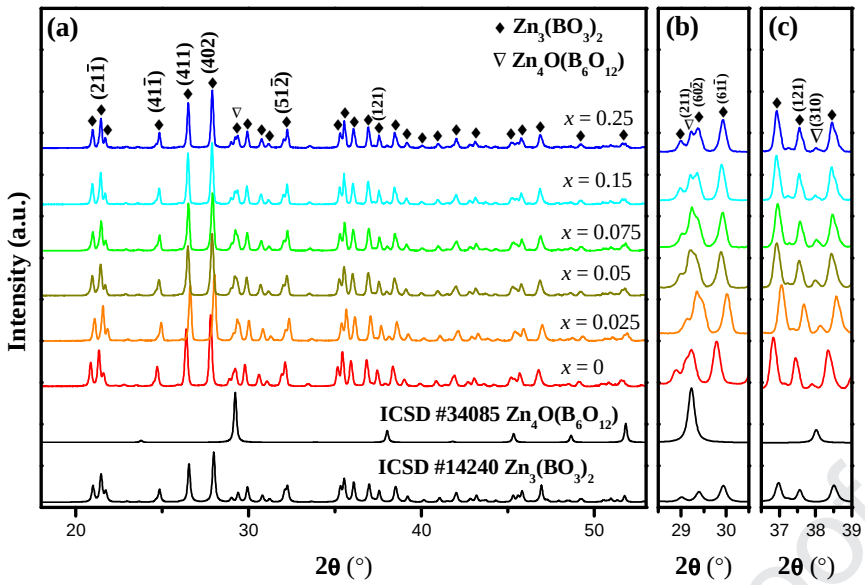

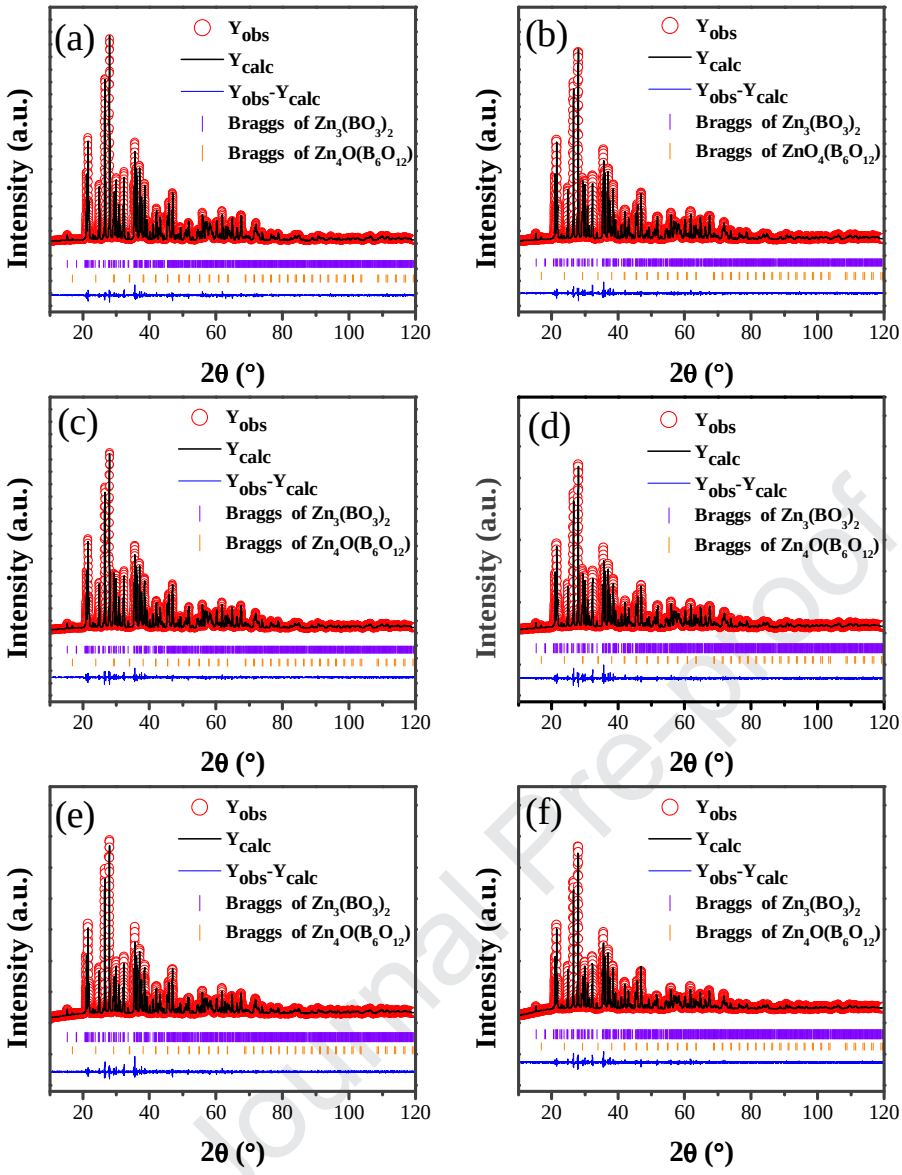

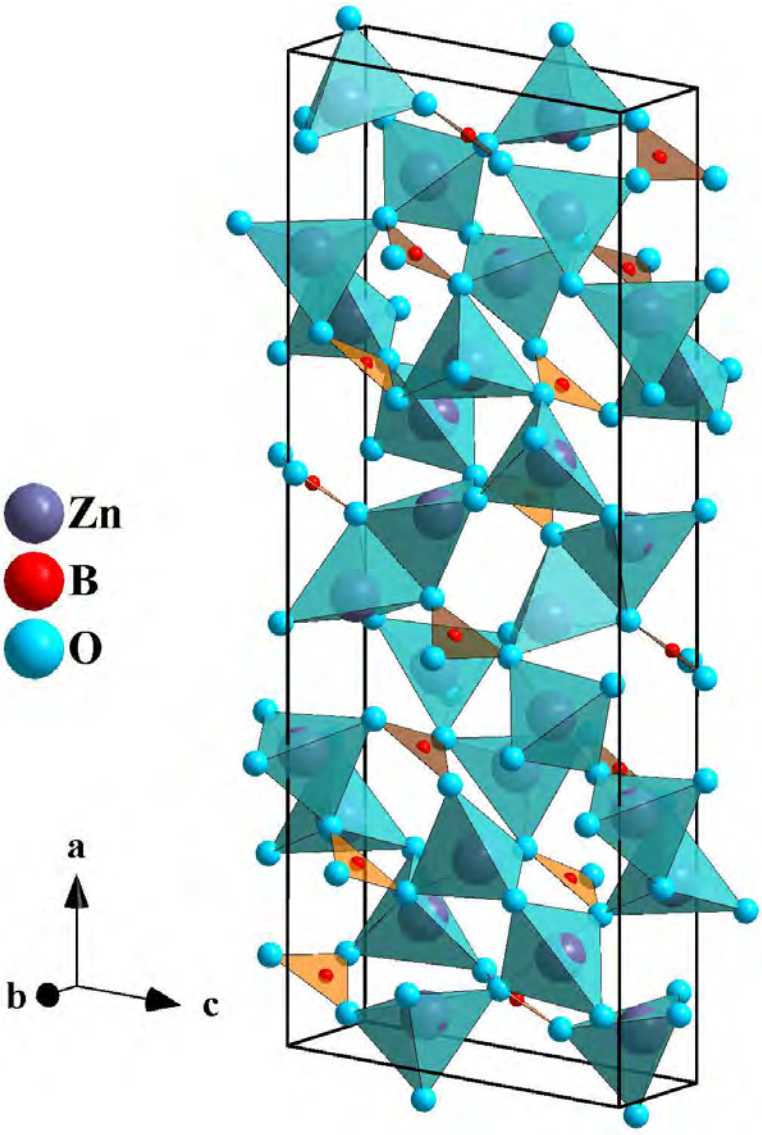

Fig.3

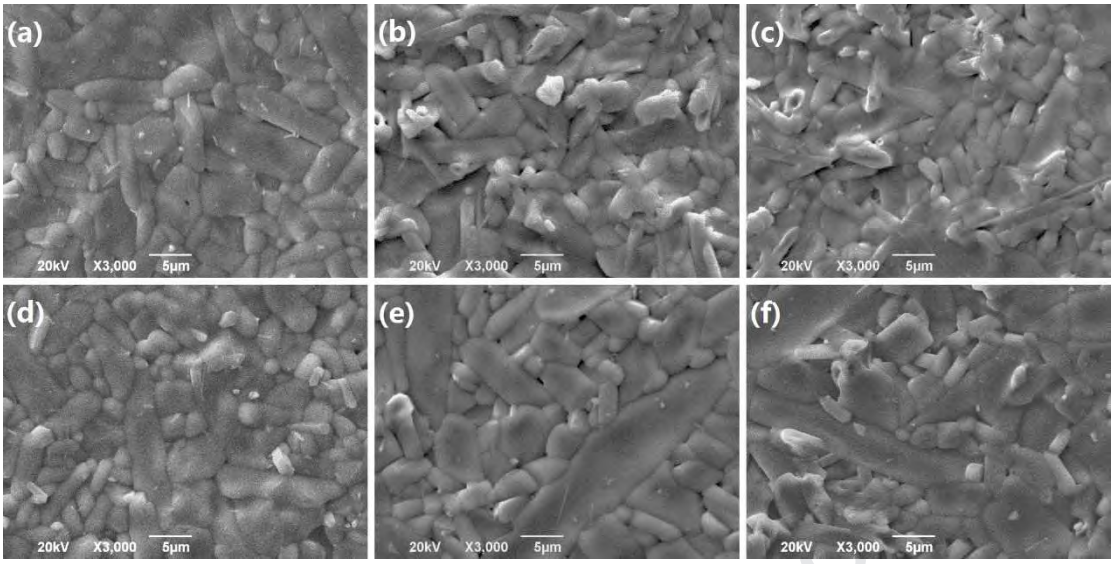

Fig.4

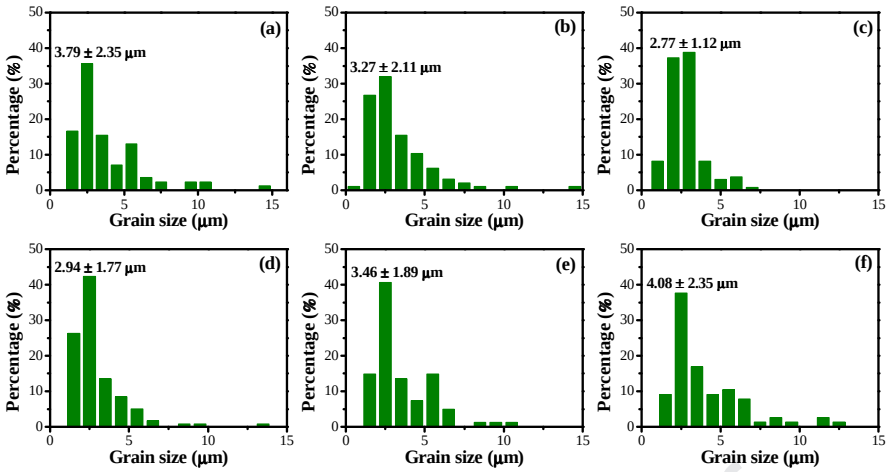

Fig.5

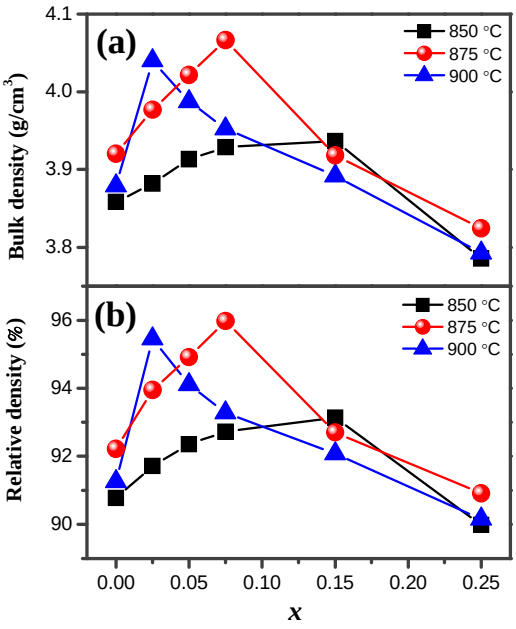

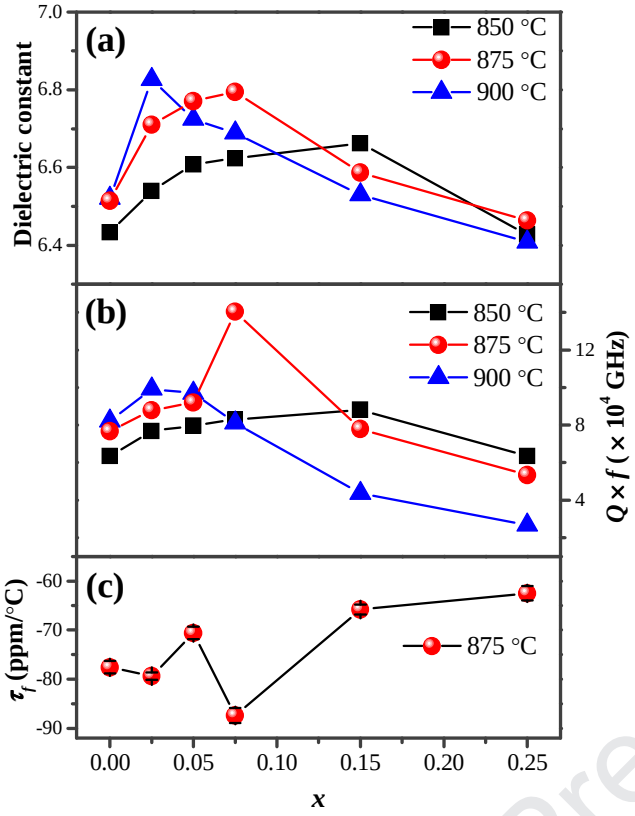

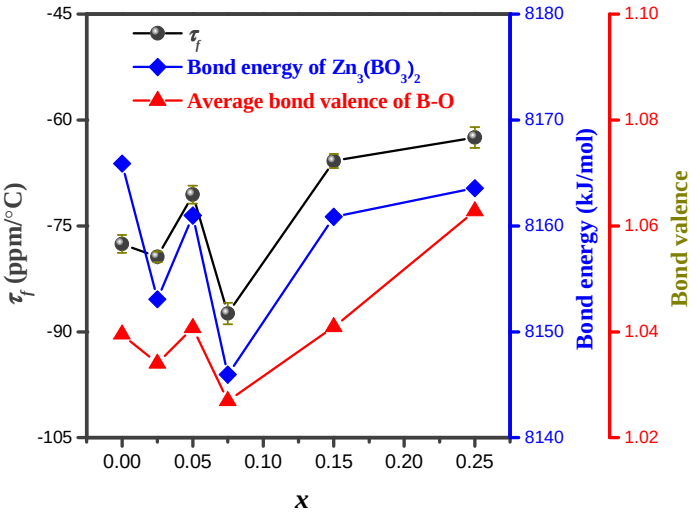

Declaration of interests

☑ The authors declare that they have no known competing financial interests or personal relationships that could have appeared to influence the work reported in this paper.

☐The authors declare the following financial interests/personal relationships which may be considered as potential competing interests: